Original Research Article

Gaussian–External Methodology Predicted Crystal Structures, Molecular Energetics, and Potential Energy Surface of the Crystalline Molecular Compass

ABSTRACT: Nanoscience, Nanotechnology, and Molecular machines have triggered the scientists of wide-ranging disciplines alike for decades now, offered the most innovative technologies to maneuver the nanoscale devices molecule by molecule. In this arena of the nano-metric world, the strategical laboratorial syntheses & computational designations of the prototype molecules/nanomaterials, and the most probable techniques for their effective functionalization always stand as mandatory credentials. Among various types of functionalizing nanomaterials, the topologically closed Si and $-(Si-O)_x-$ based dipolar crystalline macrocyclic molecular compounds exhibiting macroscopic compass/gyroscope like functions at ambient temperatures have attracted the greatest admirations. In this outlook, the research works presented herewith by employing a *Gaussian–external* methodology for the quantum mechanical characterizations of the crystal structures, computations of the molecular energetics, and derivations of the rotational potential energy surface (PES) of the experimentally synthesized difluoro- /dichloro- phenylene encapsu- lated amphidynamic/non-amphidynamic crystalline ROT–2F/ROT–2Cl siloxaalkane macrocages can be taken as a stepping stone. Under the standardized interface of *Gaussian*, we ran SCC–DFTB scheme *via* the user's script as an external program, and accessed the PES scanning techniques of the former plus the "Dispersion Energy correction" features of the latter computationally. The results reported herein are mainly found to (a) validate the X–ray produced degenerate and non-degenerate crystal structures, (b) justify the experimentally observed structural deformations of the static siloxaalkane spokes, (c) quantize the free-volume units available around the rotator, (d) disclose the energy barrier E_a to be overcome by the rotator while exhibiting 1π-flipping motion, (e) foresee the structural requisites to be adopted for designing functional crystalline free-rotors, etc. It is believed that present theoretical study enlightens us about the most essential structural and dynamical features of the gyroscopic nanostructures & molecular compasses quantitatively.

KEYWORDS: Amphidynamic Crystal, DFTB+, Dispersion-Energy, Molecular Assembly/Rotors

1. INTRODUCTION

In the recent decades, several advanced university's curricula have included multiple aspects of the computational and theoretical chemistry by realizing their extreme importance in drug discovery science, mathematical algorithms, applied science & technology, advanced artificial intelligence & machine learning techniques, etc. The massive use of them in the research fields requiring electronic structures calculations, and molecular visualizations & manipulations at the nanometer range was only recognized after the rapid development of the 3D interactive personal–computer graphics interface [1–3]. The most prospective analogies to these introductory facts can further be underscored by reiterating the Nobel Prize awardees' statement "with computer modelling, chemists are working with a third paradigm in science where the traditional combination of performing experiments with approximate theory is joined through the third partner that can enable them to perform 'exact' calculations even on the complicated, many–body systems" [1]. In fact, the exact mathematical calculations and the precise computational solutions for the simple to complex molecular systems became possible due to being the Schrodinger wave mechanical equations directly assessable *via* the basic computational techniques [2]. In the present days, such type quantum mechanical computing tasks and their exact mathematical attempts are made quite easy by means of the wide ranged software packages and the various user–friendly computer graphics [3]. One of them but, most probably a more popular and highly demanding software packages is *Gaussian*; a complete calculation scheme employed since 1970 in mainstream research [4]. Unlike others, the *Gaussian* offers relatively many more spectacular quantum mechanical features designed especially to overcome several intrinsic limitations of the analytical chemistry [4,5] along with a unique type advanced computer–aided molecular graphical interface *GaussView*; the hierarchy of research

methodologies that allows the users to set up and run almost all types of the *Gaussian* calculations virtually [3].

Among the several recognizable state-of-the-art computing abilities of the *Gaussian* software equipped with many command controlling users'-friendly '*Keywords*', the *Gaussian–external* method routed through the keyword "*External*" is most preferentially referred to the cases where computationally less expensive low–level semi–empirical yet significantly reliable type quantum computations are required by employing the priory designed external scripts [4]. Actually, this sort of the computational scheme is primarily intended to facilitate the theoretical researchers for using many other advanced–features hosting quantum chemistry program packages (external program) by utilizing a standardized interface of the *Gaussian* readily. This methodology is mainly known for its full 'Geometry Optimization' (Keyword: *Opt*) skills *via* the computational–call of the relatively better *Gaussian's* optimizer programmatically where the specifically selected external program that can feed all the required values of the mathematical functions and derivatives quantitatively is directly linked. Additionally, it enables us to implement *Opt* = *ModRedundant* functions responsible for deleting, adding, or modifying redundant internal coordinates, and the specific one character action codes such as ***A*** (Activate), ***F*** (Freeze), ***B*** (Build), ***K*** (Kill), ***S*** (Scan), etc. responsible for performing coordinate modifications, and sometimes followed by some other additional codes responsible to route the computations in a right track. For example, the relaxed Potential Energy Surface (hereafter, PES) scanning [4–6] is one of such type computational techniques where the syntaxes for the specific atom numbering or wildcards assigned to the particular type bond distance, bond angle, and/or dihedral angle followed by the action code "***S***" with controlling parameters "*nsteps stepsize*" are used. While this methodology is on the fly, the particular external program is run with a specific

energy, and optionally a dipole moment or force at each molecular geometry along with a "Text file" of the Cartesian coordinates of the immediate structure, and the user's script promptly carries out the computational tasks related to the: (a) conversion of the given text file into the "Input file" of an external program, (b) calling, running, and executing of this specific program, and (c) transformation of the results into a standard *Gaussian* "Output file" format. In other words, the Cartesian coordinates of the trial molecular geometry listed in the *Gaussian* input file format are converted into the external program's input file *via* the specifically designed user's script (the user's script inserts all the technical requisites programmatically). And, prior to initialize the *Gaussian* iterations, the same script awaits for the external (external program) calculations of electronic energies & energy gradients, and soon after being picked up of them, the *Gaussian* jobs of the user's choice are initiated.

As per the *Gaussian's* recommendation of the computationally less expensive low–level semi–empirical yet significantly reliable type quantum mechanical methods as "external program" to the *Gaussian–external* methodology, we chose "Non-self-Consistent-Charge" (hereafter, NCC–) and "Self-Consistent-Charge" (hereafter, SCC–) approaches of the extended density-functional-based tight-binding (hereafter, DFTB+) scheme [7–10] explicitly, and applied them at first to the experimentally synthesized amphidynamic type crystalline siloxaalkane molecular gyroscope ROT–2H having a non-substituted phenylene unit (rotator) encapsulated into the static yet flexible siloxaalkane spokes (stator) (Figure 1 and Figure 2) (no. of molecules/unit cell = 2 with 195 atoms in each) [11–17] with the objectives of investigating its detailed structural, and dynamical attributes. We successfully executed (a) full-geometry optimizations, and (b) PES scanning techniques with redundant dihedral angle *via* this methodology, and the concerned structural characterizations, PES derivations, molecular

dynamics (hereafter, MD) simulation at wide ranged kinetic temperatures were carried out. The concise yet comprehensive results are reported elsewhere [11, 12] along with the explicit critical assessments of the performance of NCC– and SCC– DFTB schemes. In terms of reproducing X–ray observed crystallography, determining "free–volume" unit available around the rotator, estimating rotational energy barrier E_a, predicting temperature dependent real time flipping dynamics, etc., we recognized the SCC–DFTB more precise approach. Therefore, it was selected here as an "external program", and applied its extended feature such as "Dispersion Energy correction" algorithm to address the intense van Der Waals force of interactions present in those molecular analogues that are as similar as ROT–2H but having a mobile difluoro (compass needle) (ROT–2F, no. of molecules/ unit cell = 4 with 195 atoms in each) (Figure 1(a)), and a static dichloro (ROT–2Cl, no. of molecules/unit cell = 2 with 195 atoms in each)) substituted phenylene unit (Figure 1(b)) centrally in their orthorhombic crystals, and explored their experimentally observed unit–cell structures followed by the complete structural interpretations of their geometrical deformations, rotational PES, and the corresponding degenerate equilibrium unit–cell structures (the flipped structural positions) theoretically. To our experience, accomplishing such type complex theoretical calculations just by utilizing significantly low computational resources yet producing quite reliable and precise quantitative results were almost impossible by executing either of the *Gaussian* or the SCC–DFTB alone schemes as the former one was unable to terminate the computational procedures normally time to time, but fortunately hosts the PES scanning computational technique (*ModRedundant*) at each desired structural parameter constrained to the specific value, whereas the latter lacks the same type computational features despite producing semi–empirical level results even by assessing its computationally

challenging and demanding "Dispersion Energy corrections" features. Therefore, the facile interlinking and the effective execution of both of them *via* the "*Gaussian*−

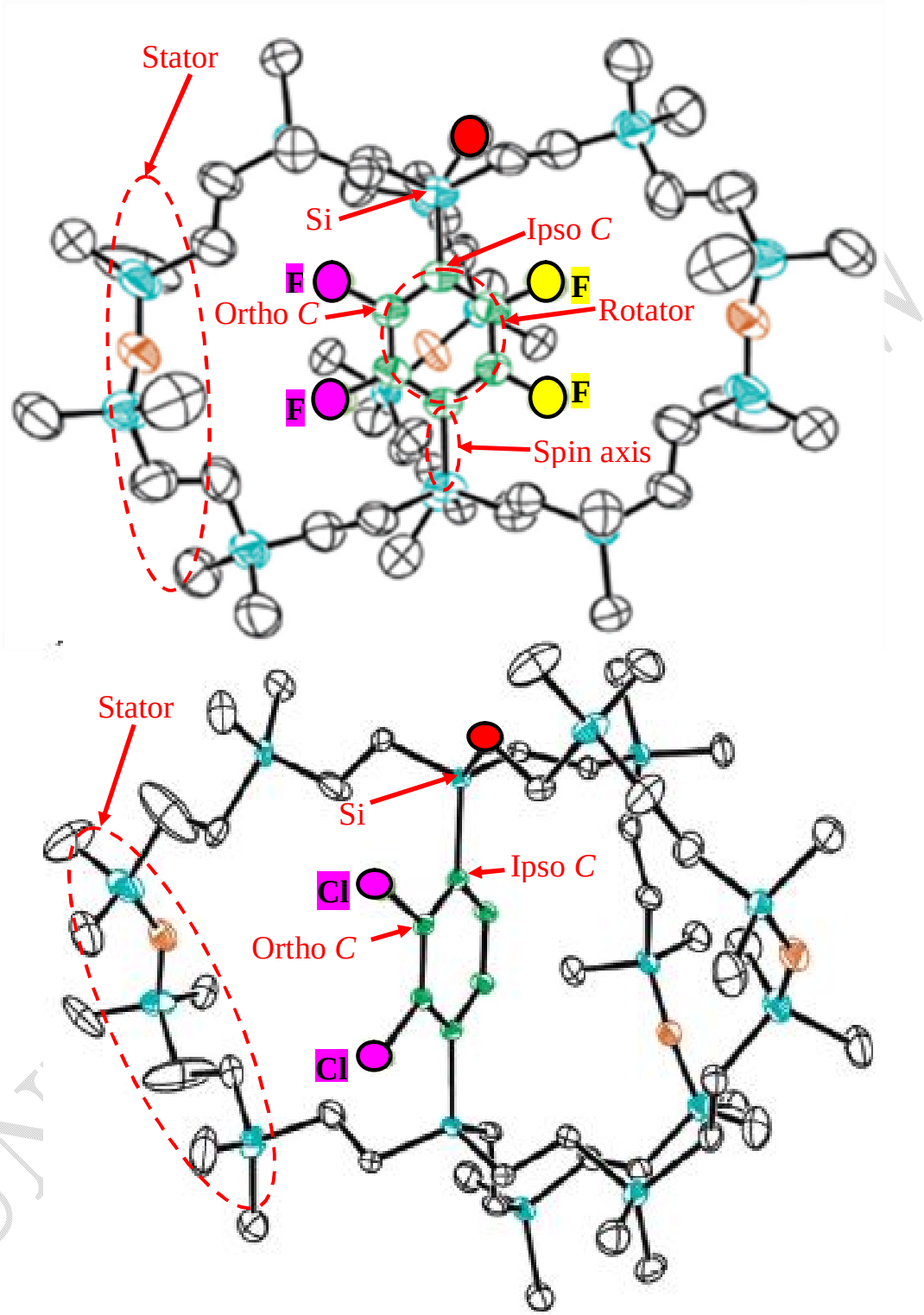

Fig.1. An X–ray crystallography of the experimentally synthesized crystalline siloxaalkane molecule (a) ROT–2F (molecular compass) with two stable positions **B** and **B'** of the difluorophenylene rotator (indicated by yellow and pink spheroids), (b) ROT–2Cl with a single stable position of dichlorophenylene (indicated by pink spheroids). Both of them are reproduced from the ref. 14. Hydrogen atoms and the structural disorder of the siloxaalkane chains are omitted for clarity. The phenylene dihedral angle ϕ in both of them are formed by the **C** atom of the arm (red spheroid), **Si** atom of the spin axis (blue), *ipso* and *ortho* **C** atoms of the phenylene (green).

external" methodology became the most suitable option for us in order to cope with the giant crystalline molecular assemblies of ROT–2F & ROT–2Cl, and their predominant inter-/intra-molecular interactions. Meanwhile, all the theoretical investigations conducted herewith with the extremely low computational resources are believed as quite indispensable in order to understand the unique amphidynamic features of the crystalline molecular compasses owing to the functionalizations in nanotechnology such as (a) inventing ambitious yet realistic type smart, responsive, and intelligent nanomaterials, (b) demonstrating externally controlled rotary motion by conserving internal volume, (c) recognizing completely unidirectional type molecular rotation throughout the application of electric/magnetic fields, light, and many other external stimuli [18–20], (d) functionalizing experimentally observed dichroism and birefringence type optical properties [15,18,19], (e) realizing functional crystalline free rotors (molecular machine) at room temperature, etc. With this, the contents of the research article are organized as: in section 2, the detailed Theoretical approaches and Computational methods are expressed; in section 3, the Results and the relevant Discussions are presented, and in section 4, the concise Conclusions are outlined.

2. Material and Methods

As per the X–ray observed crystallography reported elsewhere [14] by Setaka *et al.* in 2010, the orthorhombic crystal of ROT–2F (number of molecules per unit cell = 4) at 273K behaves as a molecular compass due to undergoing self-1π-flipping of its difluoro substituted dipolar phenylene rotator (compass needle) along the **C–Si** spin axis linked directly to the three static siloxoalkane arms: the two degenerate unit-cell structures, hereafter assigned the code **B** to the one having a specific dihedral angle (the atoms involved in forming the dihedral angle are

defined in Figure 1 and Figure 2) $\phi = 0.56\pi$, and **B'** to the next having $\phi = 1.57\pi$; whereas the orthorhombic crystal of ROT–2Cl (number of molecules per unit cell = 2) with a rigid dichlorophenylene unit ($\phi = 0.61\pi$) behaves as a non–amphidynamic type at the same temperature. The respective crystallographic information files with *.cif* extension were accessed directly through the Mercury Crystallographic software [21(a)], and the corresponding X–ray derived unit-cell coordinates of the ROT–2F (structure **B** & **B')**, and ROT–2Cl were extracted explicitly, and used them as their trial unit-cell coordinates in the *Gaussian* text file format for the *Gaussian–external* optimization procedures. This particular geometry optimization task for the ROT–2Cl was just carried out here for the sake of theorizing experimentally observed structural deformation of its surrounding siloxaalkane spokes, and interpreting the effect of its bulky substituents such as **Cl** on the phenylene ring to the latter. Beside this, the optimized structure of the ROT–2Cl unit-cell was referred here to characterize the crystal structure of the ROT–2F quantitatively. All the ground state equilibrium structures (both experimental and theoretical) were rendered in the 3D space by *Jmol* software [21(b)], and the corresponding structural parameters such as bond lengths, bond angles, dihedral angles, free–volume units, etc. were explicitly measured. While scanning the rotational-PES of the ROT–2F molecular compass in respect to its predefined dihedral angle ϕ through the *Gaussian–external* under "PBC + Dispersion Energy Correction" features of the SCC– DFTB, the *Gaussian* action code "***S***" followed by its controllers "*nsteps stepsize*" were used, and computed the concerned electronic energy at each specific ϕ (Keyword: *ModRedundant*) scaled up by the *stepsize* +2° (clockwise) and –2° (anticlockwise) from the $\phi = 0.44\pi$ (modulo π) of the pre-optimized structure of **B**. This particular computation was actually needful for determining the exact energy barrier E_a experienced by the central difluorophenylene rotator, and for revealing the reasons underlying its

facile rotation even at a temperature as equal as 298K (room temperature); either of them were experimentally unpredictable but thought as the indispensable indicators for exploring temporal rotary motion quantitatively. In the case for ROT–2Cl, the same type PES calculation was inapplicable due to its experimentally confirmed non–amphidynamic behavior.

The “Input file” for the external program SCC–DFTB was prepared by inserting the specific "Keywords" programmatically *via* the user's external script. The script that can command the concerned 'quantum mechanical calculations' was written on the basis of DFTB+ manual available elsewhere [22]. The Hamiltonian and the associated parameters were configured through the "Hamiltonian = DFTB", and the particular type crystalline conditions were imposed by "*Periodic = Yes, & Lattice-Opt = Yes*" functions. The Brillouin zone integration was specified *via* the special *k*–points and their weights in integral under "*KPointsAndWeights*", and was followed by the explicit sets of the X–ray derived lattice vectors of the ROT–2Cl and ROT–2F. The entire molecular reorientations that cause to break the symmetry during *Gaussian* iterative procedures were blocked by “*NoSymm*” keyword. The Cartesian coordinates of the trial structure of each specific unit-cell were mentioned in the *XYZ* format under the controlling tag "*Geometry = GenFormat*". The geometry component "*AppendGeometries = Yes*" that creates a Cartesian coordinate file with all the recurring geometries needful for the continuous monitoring of the normal computations was set, and the "*SCC = YES*" procedure was called to ensure the SCC type calculations. The "*SCCTolerance*" and "*MAXSCCIterations*" were slightly loosened to the standard of $1e{-}4$ and 200 respectively so as to achieve the successful terminations of the computational procedures even with low computational resources. The inter– /intra– molecular interactions in the crystal were taken into account by executing "*Dispersion = SlaterKirkwood*" (Slater– Kirkwood polarization atomic

model [22, 23]) functions, and the required dispersion constants such as polarizabilities α (Å^3), Slater–Kirkwood effective numbers N_{eff}, cutoff interaction range r_c (Å), and the effective charge (*Chrg.*) for each and every atoms with unique coordination were supplied through the "*HybridDependentPol*" tag. The concerned parameter sets for the **H**, **C**, **O**, and **Si** atoms were taken from the previous publications of the same authors [11, 24, 25] where every parameter was properly validated and tested in reference to ROT–2H. The dispersion constants

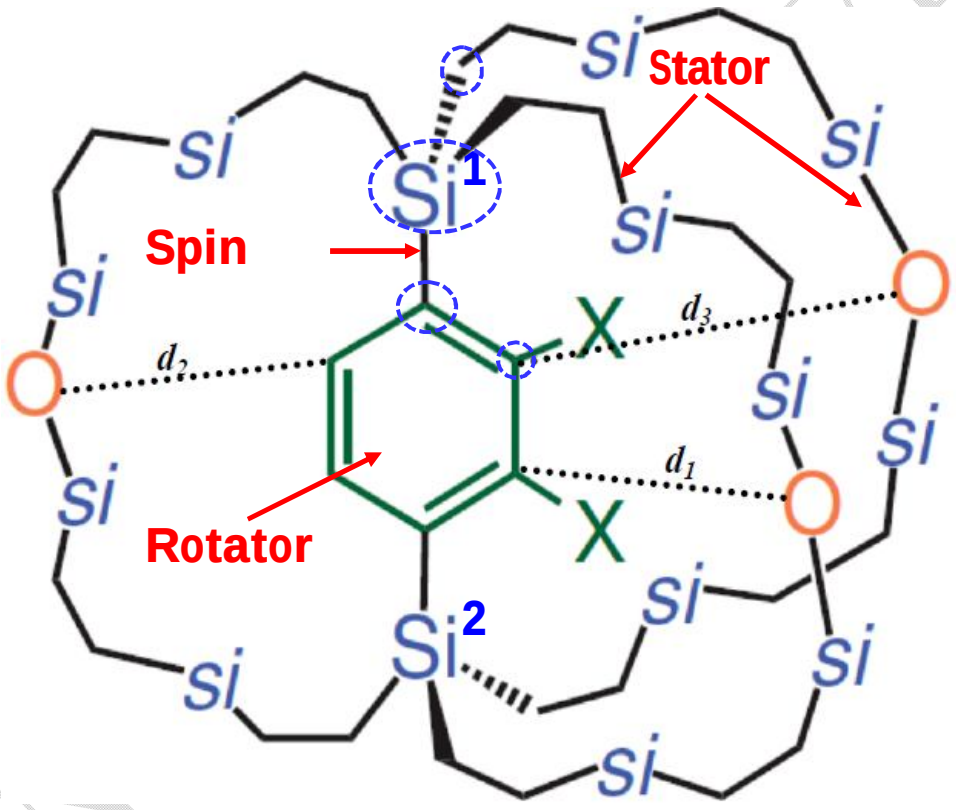

X = H (ROT–2H)
X = F (ROT–2F)
X = Cl (ROT–2Cl)

Fig. 2. A sketch showing a completely closed structural topology of the siloxaalkane molecular compass. The two methyl (CH_3) groups attached to each **Si** atom of each siloxaalkane arm are omitted for clarity. The substituent "**X**" represents either **H** (ROT–2H), **F** (ROT–2F), or **Cl** (ROT–2Cl). The set of the distances d_{CO} = {d_1, d_2, d_3} approximates the free-volume unit available around the central phenylene rotator, and the atoms encircled by the blue dotted spheroids define the actual dihedral angle(ϕ).

for **F** and **Cl** atoms were determined mathematically as mentioned elsewhere [26, 27], and the required Slater–Koster files with a focus on solid state systems were explicitly used from the *mio–1–1* and *pbc–0–2a* sets for every pairwise permutation atomic types [22, 28].

3. Results and Discussions

3.1 Crystal Structures and Energetics of the Siloxaalkane Molecular Compass

As mentioned in the "Introduction" and "Computational Details" sections, the SCC–DFTB calculations with 'dispersion energy corrections' became the authors' most preferable computational scheme as the *Gaussian–external* executed external program. The

promising yet computationally low-cost features of the DFTB that suit for the present methodology designed

Table 1. Experimental vs. Theoretical structural parameters for the molecular compass **ROT–2F** and a reference molecular crystal **ROT–2Cl** in their unit cell structures.

Crystalline Molecular Compass/co-mpounds	Chemical bonds associated with the central dihalo substituted phenylene	X–ray (Experiment; *Expt.*) and *Gaussian–external* with "SCC–DFTB + PBC + Dispersion Energy correction" (Theoretical; *Th.*)					
		Bond Length (*nm*)		"Free –Volume" d_{CO} $\{d_1, d_2, d_3\}$ (*nm*)		Phenylene dihedral angle ϕ (π)	
		Expt.	*Th.*	*Expt.*	*Th.*	*Expt.*	*Th.*
ROT–2F Position **B**	C–C C–F C–H C–Si_1 C–Si_2	0.136 0.144 0.093 0.189 0.189	0.141 0.137 0.110 0.188 0.188	 0.591 0.584 0.844	 0.553 0.579 0.859	0.56	0.44
Position **B'**	C–C C–F C–H C–Si_1 C–Si_2	0.137 0.150 0.093 0.189 0.189	0.139 0.141 0.110 0.187 0.187	 0.589 0.589 0.844	 0.589 0.594 0.845	1.57	1.44
ROT–2Cl	C–C C–Cl C–H C–Si_1 C–Si_2	0.139 0.176 0.093 0.191 0.189	0.140 0.141 0.110 0.187 0.187	 0.705 0.786 0.795	 0.678 0.794 0.798	0.61	0.64

especially to characterize the crystalline molecular geometry, and to compute the most essential descriptors associated with the rotary dynamics of the experimentally synthesized crystalline heteroatomic molecular compass ROT–2F where charge balance between the atoms is very crucial include; (a) comprehensive incorporations of the self-consistent redistribution of the Mulliken atomic charges during the entire computational procedure; (b) in–depth derivations of the required nuclear forces by taking the derivatives with respect to the nuclear coordinates; (c) detailed descriptions of the long range molecular interactions with empirical type dispersion constants *via* the Slater–Kirkwood polarization atomic model. In this study, the X–ray derived nuclear coordinates of the two degenerate equilibrium structures **B** and **B'** of the ROT–2F, and a single stable structure of the ROT–2Cl were optimized at first under PBC + Dispersion Energy correction features, and characterized their crystalline geometries in reference to their X–ray derived unit-cells. The respective low energy structures rendered through the *Jmol* are displayed

in Figure 3(b),

Figure 4(b), and Figure 5(b) respectively, and are compared quantitatively with the X–ray crystallographic structures shown in Figure 3(a), Figure 4(a), and Figure 5(a). In order to specify each of these unit-cell geometries in the 3D space, we set the mostly responsible geometrical parameters such as bond lengths, bond angles, dihedral angles, free–volume units, etc., and measured them explicitly. As shown in Table 1, all the phenylene C−C bond lengths are theoretically estimated as 0.141*nm* in average: a distance longer than the standard C=C bond (length = 0.134*nm*) but shorter than the standard C−C bond (length = 0.147*nm*); indicates the presence of partial double bond characters in the dihalo substituted phenylene units of both ROT–2Cl and ROT–2F. Accordingly, the closed investigations of the concerned interior and the exterior bond angles of their phenylene units and their critical comparisons with the corresponding bond angles measured in the regular planar benzene (bond angle = 120°) molecule signify the existence of notably varied angular distortions. Both of these electronic and structural irregularities are caused by the intense effect of the van Der Waals type intra– and inter–molecular interactions experienced by the phenylene units: the phenylene units of them feel strong force of interactions with their surrounding siloxaalkane spokes (intra–molecular) themselves are interacted with the neighboring molecules (inter–molecular) arranged periodically in the crystalline state. The origination of such type nonbonding interactions is mainly caused by the structural congestion

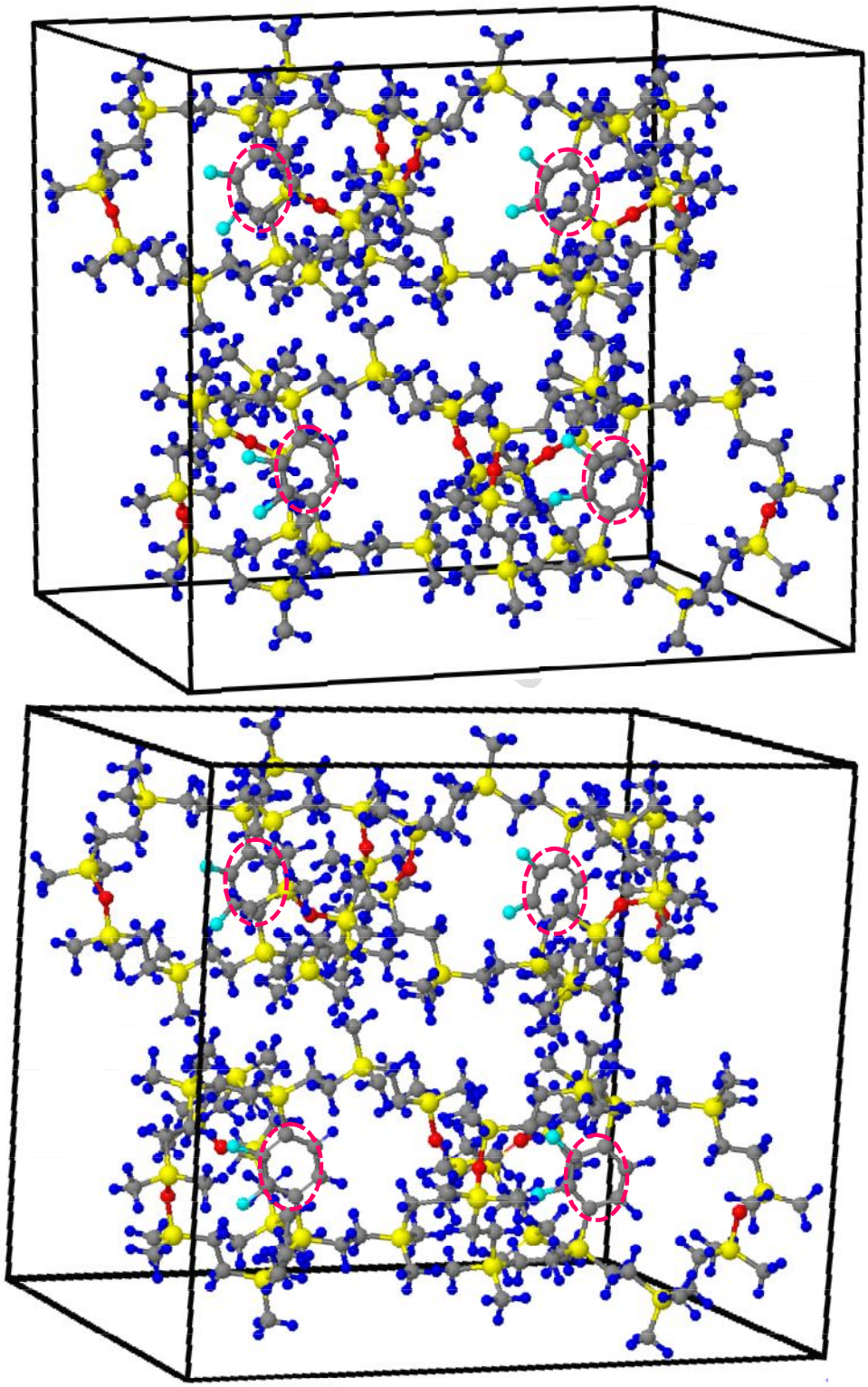

Fig.3. (a) X–ray crystallography (orthorhombic crystal with four molecules per unit cell), (b) *Gaussian-external* with "SCC–DFTB + PBC + Dispersion energy correction" optimized unit-cell geometry (structure **B**, $\phi = 0.44\pi$) of the crystalline siloxaalkane molecular compass ROT–2F. The cyan, blue, gray, red, and yellow spheroids represent F, H, C, O, and Si atoms respectively. Each difluorophenylene rotator in both of the unit-cells is enclosed by the red

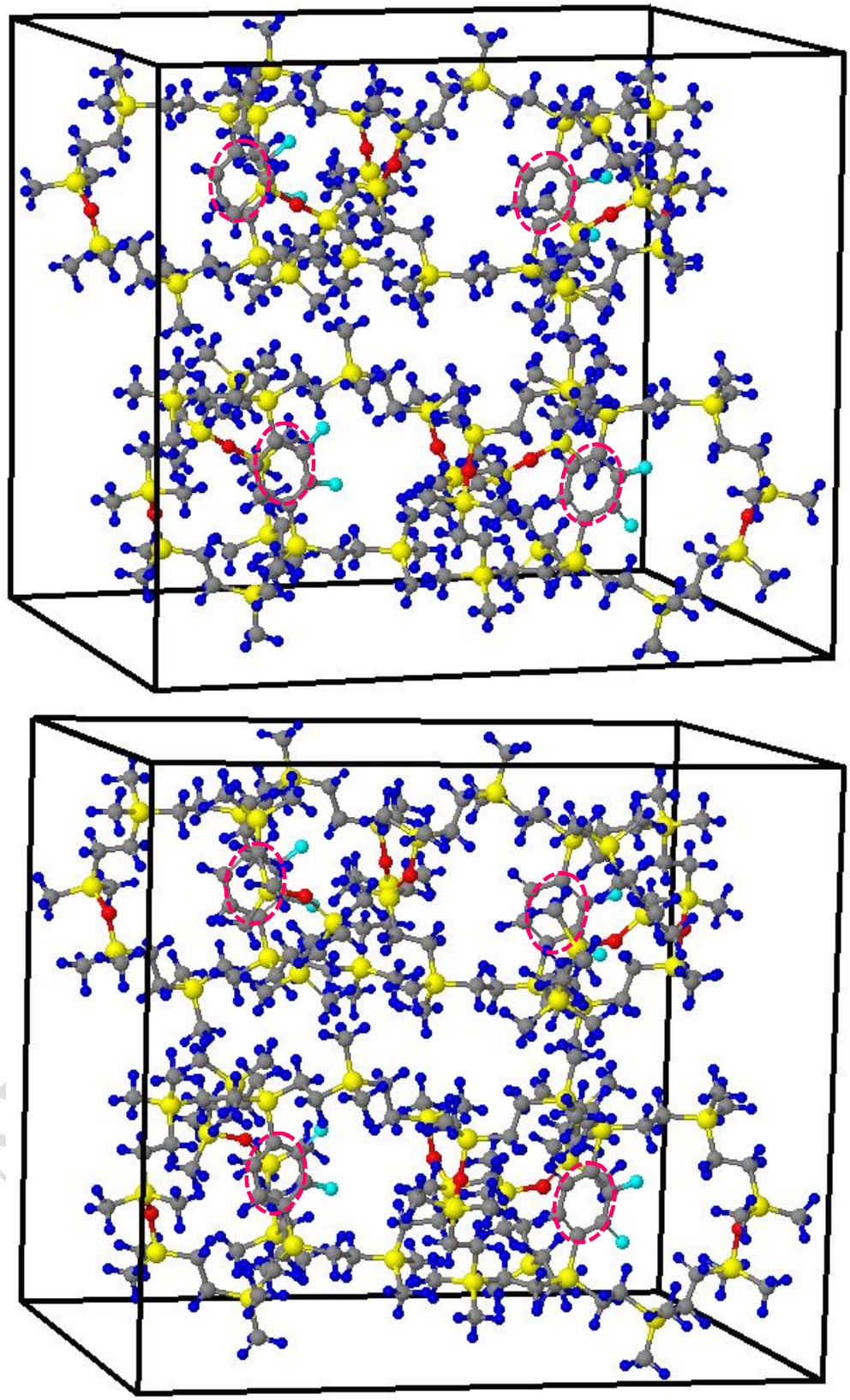

Fig.4. (a) X–ray crystallography (orthorhombic crystal with four molecules per unit cell), (b) *Gaussian-external* with "SCC–DFTB + PBC + Dispersion energy correction" optimized unit-cell geometry (structure **B'**, ϕ = 1.44π: a 1π flipped structure of **B**) of the crystalline siloxaalkane molecular compass ROT–2F. The cyan, blue, gray, red, and yellow spheroids represent F, H, C, O, and Si atoms respectively. Each difluorophenylene segment in both of the unit-cells is enclosed by

created steric hindrance which in fact is responsible for imposing the central phenylene units to occupy a particular site into the free space present inside the strategically designed/synthesized peripheral siloxaalkane spokes. Besides these structural interpretations underlying the central dihalo phenylene units, the theoretically predicted dihedral angles ϕ with respect to the peripheral arm (as defined in Figure 1(a) and Figure 1(b)) support their irregular shapes in both ROT–2F and ROT–2Cl: the dihedral angles ϕ measured in the X–ray produced structures **B** and **B'** of the former $0.56\pi \leftrightarrow 1.57\pi$ (1π flip) are theoretically converged to $0.44\pi \leftrightarrow 1.44\pi$ (1π flip), and that for the latter, $\phi = 0.61\pi$ is converged to 0.64π. Energetically, the theoretically derived electronic energy of the structure **B** ($E = -704.278668\ E_h$) is found exactly equal to that of the **B'** ($E = -704.278668\ E_h$); reassuring the experimentally determined ratio of their site occupancy factors and their identical number density [14, 15] (**Chart 1**), and that for a single stable equilibrium structure of the ROT–2Cl is $E = -352.602281\ E_h$. In reference to all of these theoretically derived structural and energy datasets, the X–ray observed degenerate equilibrium structures **B** and **B'** of the ROT–2F related to each other by 1π difluorophenylene flipping, and a similarly observed single low energy equilibrium structure of the ROT–2Cl are confirmed.

In addition to verifying this energetic degeneracy, the experimentally observed deformed type siloxaalkane spokes in ROT–2F and ROT–2Cl are validated theoretically herewith by estimating their respective free–volume units; a space where the centrally enclosed dipolar substituted phenylene rotator is residing inside which it demonstrates either the facile flipping motion conveniently as in ROT–2F or the restriction in flipping as in ROT–2Cl. In principle, greater the structural deformation narrower is the free–volume units, and bulkier the substituents attached to the central rotary unit more is the structural dislocation of the peripheral siloxaalkane arms, and themselves are the most potential means on the basis of which many other structural

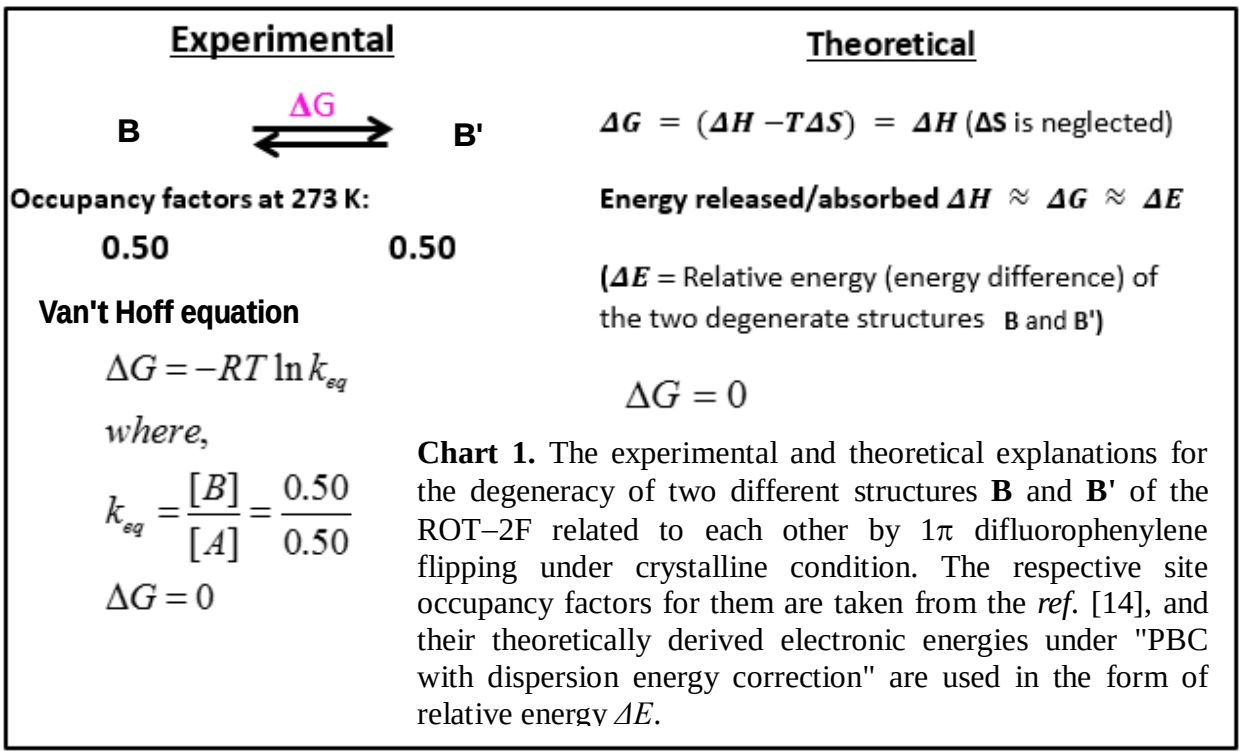

Chart 1. The experimental and theoretical explanations for the degeneracy of two different structures **B** and **B'** of the ROT–2F related to each other by 1π difluorophenylene flipping under crystalline condition. The respective site occupancy factors for them are taken from the *ref.* [14], and their theoretically derived electronic energies under "PBC with dispersion energy correction" are used in the form of relative energy ΔE.

and dynamical assets of the ROT–2F compass such as rotational potential energy surface (hereafter, PES), rotational energy barriers, types of the rotary motion (facile, restricted, or prevented), temporal behavior of the rotating segment, flipping rates of the central rotator, etc. can be interpreted. Since both free–volume units and the degree of structural deformations play decisive roles in exhibiting either the smooth or the restricted type rotary motion, we have emphasized these descriptors here quantitatively on the basis of which the theoretically derived crystal structures of both ROT–2F & ROT–2Cl are presented, and validated with the corresponding descriptors measured in the experimentally derived crystal structures. Actually, both of them possess a significantly better and a robust type Si–based siloxaalknae spokes with Si–O–Si segments as their static framework, the Si–O bond stretching features plus the Si–O–Si bending degrees of freedom make these spokes flexible and deformed. Herein, we have integrated all of these structural analogies *via* the set of the distances $d_{CO} = \{d_1, d_2, d_3\}$ (Figure 2)

measured explicitly in all the X–

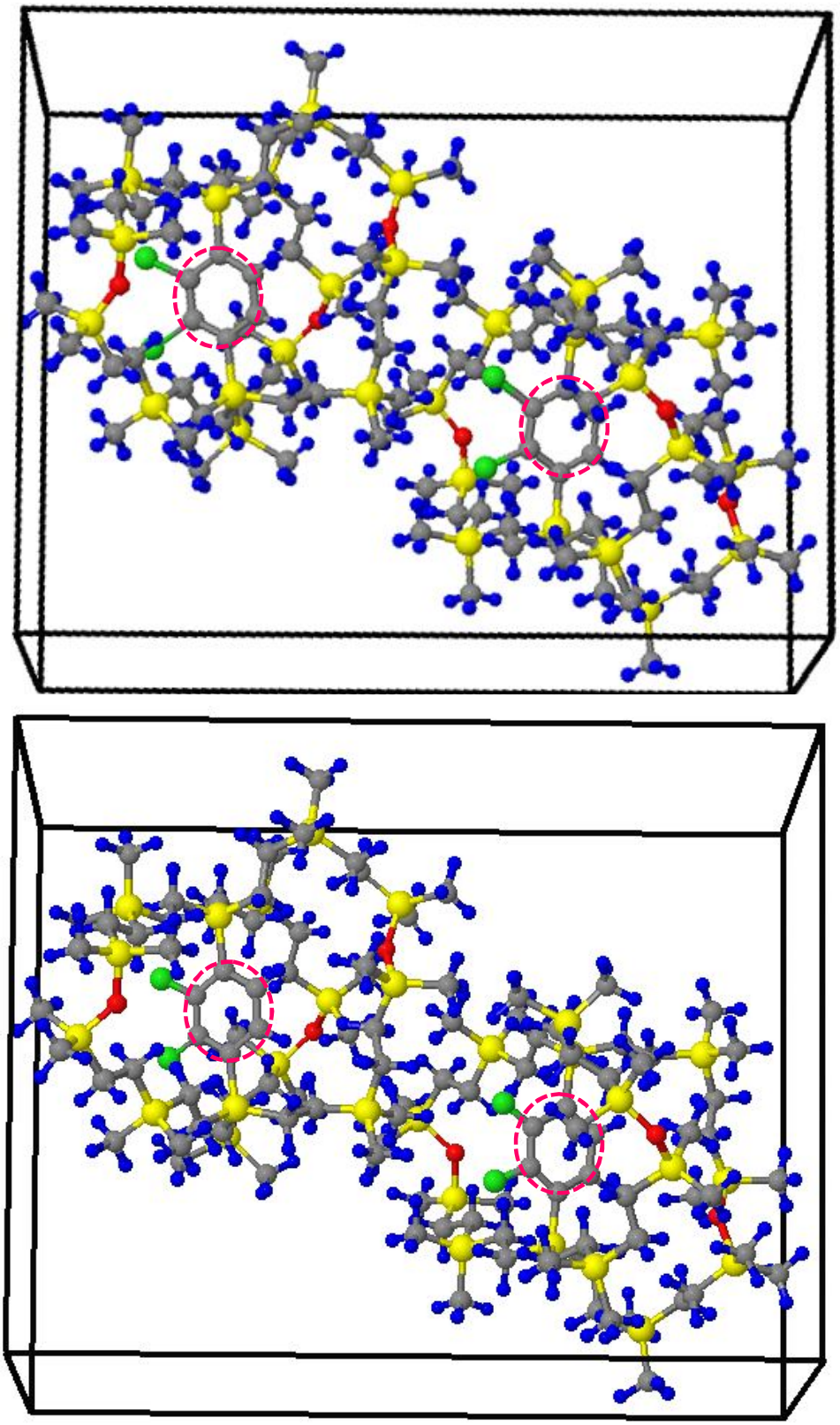

Fig.5. (a) X–ray crystallography (orthorhombic crystal with two molecules per unit cell), (b) *Gaussian-external* with "SCC–DFTB + PBC + Dispersion energy correction" optimized unit-cell geometry of the crystalline siloxaalkane molecule ROT–2Cl. The green, blue, gray, red, and yellow spheroids represent Cl, H, C, O, and Si atoms respectively. Each dichlorophenylene segment in both of the unit-cells is enclosed by the

ray derived and the theoretically optimized unit cell geometries as listed in Table 1. The d_{CO} = $\{d_1,$

$d_2,\ d_3\}$ datasets in fact approximate the intervening space exists in between **O** atom of each siloxaalkane arm and the phenylene *ortho* **C** holding halogen atom, and therefore, are considered here as the most precise mean of theorizing free–volume units quantitatively. We found all those explicit values measured in the respective X–ray and theoretically derived equilibrium unit cell structures quite consistent to each other; guarantying the maintenance of experimentally observed free–volume units even in the theoretically produced equilibrium structures without undergoing the breakage of closed gyroscopic/compass-like architectures. The increasing trend

Table 2. Experimental vs. Theoretical structural parameters for each siloxaalkane arm of the crystalline molecular compounds **ROT–2F** and **ROT–2Cl** in their unit cell structures.

Crystalline Molecular Compounds	X–ray (Experiment; *Expt.*) and *Gaussian–external* with "SCC–DFTB + PBC + Dispersion Energy correction" (Theoretical; *Th.*)				
	Si–O–Si angle (θ) (π)		**Bonds**	**Bond lengths (*nm*)**	
	Expt.	***Th.***		***Expt.***	***Th.***
(ROT–2F) Structure **B**	0.960 0.840 0.840	0.777 0.801 0.758	C–C C–H C–Si Si–O	0.150 0.096 0.189 0.159	0.152 0.110 0.188 0.165
Structure **B'**	0.967 0.834 0.834	0.801 0.768 0.762	C–C C–H C–Si Si–O	0.150 0.096 0.189 0.159	0.152 0.110 0.188 0.165
(ROT–2Cl)	0.801 0.801 0.860	0.745 0.795 0.761	C–C C–H C–Si Si–O	0.151 0.110 0.180 0.170	0.153 0.110 0.188 0.176

of each set of the $d_{CO}\{d_1,\ d_2,\ d_3\}$ value measured for ROT–2F and ROT–2Cl reflects that the latter possesses a relatively larger amount of free–volume than that by the former; illuminates the

existence of maximum amount of structural deformation (dislocation of the peripheral arms) in the latter's siloxaalkane spokes. The detailed comparison with the similar datasets measured for ROT–2H, and its contrastingly low structural deformation relative to both ROT–2F and ROT–2Cl are reported elsewhere [16, 25] by the same authors without using "Dispersion Energy Correction" features of the DFTB. This trend of the d_{CO} further signifies that the bigger halogen atoms such as **Cl** (atomic size (covalent radius $R_{cov.}$) = 0.99Å) attached to the central phenylene unit of ROT–2Cl makes it bulkier (dichlorophenylene unit needs a more free- volume inside the spokes) than that by the relatively smaller **F** (atomic size (covalent radius $R_{cov.}$) = 0.64Å) atoms attached to the central phenylene unit of ROT–2F (the difluorophenylene unit needs relatively a less amount of free–volume), and the bulkier dichlorophenylene unit always pushes the surrounding siloxaalkane spokes outward (ballooning) in a greater extent than that by the less bulky difluorophenylene. The relatively more structural deformations observed more especially in ROT–2Cl is again due to the stronger steric effects of its bulkier dichlorophenylene segment to the surrounding siloxaalkane spokes; a complementary electronic effect responsible to maintain both of the "just–required" or "more than required" amount of free-volume units by attaining the gyroscopic/compass-like framework with completely closed structural topology. The same are the reasons why many experimentalists/theoreticians tend to give full attentions towards unique strategical designation and the efficient laboratorial syntheses of the macrocyclic molecular rotors/gyroscopes/compasses with flexible yet robust type macrocages that can dilate inwards and outwards in the course of accommodating flipped positions (flipping motion) of the substituted or the non-substituted type phenylene rotators centrally so as to achieve; (a) a substantially weaker steric hindrance and an extremely low intramolecular type interactions between the rotating unit & the surrounding frameworks, (b) a completely closed structural

topology with just enough free-volume units, (c) a remarkably lower rotational hindrance/energy barrier E_a, (d) a facile flipping motions of the central rotator even at the temperature as equal as 298 K (room temperature), (e) a well-controlled electrical, thermal, and optical functionalizations, etc. The detailed about these descriptors and their decisive roles in exhibiting molecular gyroscopic/compass-needle functions readily and effortlessly is given in the subsection 3.2.

One of the most significant causes that can deform the peripheral siloxaalkane spokes of the ROT−2F (structure **B** and **B'**) and ROT−2Cl is use of the flexible and stretching type −(Si−O)$_x$− bonds, and their chains & segments in constructing their frameworks even though the latter were given first preference for functionalizing them externally rather than creating topologically closed framework [13,14]. Therefore, all the bonding parameters associated with these segments such as Si–O–Si bond angle (θ), and C–C, C–H, C–Si, Si–O bond lengths of each peripheral siloxaalkane arm are subjected to change. The same is the reason behind taking account into them here mainly for the complete theoretical characterizations of the crystal structures, and the related structural & dynamical attributes. These parameters measured in the *Jmol* rendered graphical models of both of the X–ray and *Gaussian–external* derived unit cells are listed in Table 2. These structural datasets are also referred here for justifying the free–volume units confirmed earlier with the theoretically computed $d_{CO}\{d_1,\ d_2,\ d_3\}$ datasets. While inspecting all these bonding parameters closely, no big variation and the notable changes in bond lengths are observed in almost all the covalent bonds linked with the **C** atom, whereas the theoretically predicted bond lengths and bond angles associated with the **Si** atom, and its −(Si−O)$_x$− chains & Si−O−Si linkages are deviated from their values measured in the X–ray derived unit cells. But, in regard to their partial ionic and double bond characters caused by the delocalization of lone pair electrons on the O atom into the vacant π^* or d orbitals of **Si** (the

Si–O bond is 75% covalent and 25% ionic [29]), the diverseness appeared on the Si−O−Si bond angles and $-(Si-O)_x-$ bond lengths in quantum mechanically optimized unit cells of both of the ROT–2F and ROT–2Cl are theoretically acceptable as this sort of the electronic effects are only addressed through the quantum mechanically approximated yet computationally implementable mathematical formulations and derivations [30] in the theoretical models. Except few of these notable structural abnormalities between the experimentally and theoretically derived unit cell geometries, the 3D positional alignment and the spatial distribution of each siloxaalkane arm, and their Si–CH_3, Si–O, Si–C, C–H, etc. segments in each molecule of the unit-cell are found to be quite satisfactory. The authors suggest to the interested researchers for consulting with the concerned datasets of ROT–2H reported by us elsewhere [11] for the detailed impacts of the steric effect imposed by the bulky dihalo groups of the ROT–2Cl and ROT–2F. For now, we shortly summarize here as the steric hindrance imposed by the dihalo groups on the central rotator makes the surrounding siloxaalkane arms outward–dilated which eventually not only diminishes their respective Si–O–Si angles towards acuteness but also enlarges the corresponding $d_{CO}\{d_1, d_2, d_3\}$ values (free–volume unit) with outward expansion of the entire spokes.

After all these critical structural overviews and the geometrical analogies, the remarkable consistencies in the unit-cell geometries produced through the *Gaussian–external* methodology operated SCC–DFTB with "Dispersion Energy correction" under PBC scheme (Figure 3 to Figure 5) underscore its outstanding computing abilities and the precision levels even at the exceptionally low computational resources platforms. All the concerned results and the relevant discussions reported here have called full attentions to the DFTB+, and its extended

computational & theoretical features bestowed to the solid state molecular assemblies as well as to its standalone applications in the theoretical research fields.

3.2 Interpretation of the Rotational Potential Energy Surface (PES)

As explained by Setaka *et al.* in their in–depth experimental reports available elsewhere [14], the orthorhombic type crystals of ROT–2F and ROT–2Cl behave as an amphidynamic and non–amphidynamic type respectively at T = 273K: the former one has a mobile and the latter one has an immobile type difluoro– and dichloro– substituted phenylene segments respectively inside the free-volume units maintained strategically through the chemically identical robust, static, yet flexible type Si–O based slioxoalkane spokes (Figure 1). According to their X–ray observations, the ROT–2F attains two stable degenerate type equilibrium structures **B** and **B'** with the respective dihedral angles (ϕ) 0.56π and 1.57π (the atoms involved in forming the concerned dihedral angle ϕ are defined in Figure 1) related to each other by 1π flipped positions of the difluorophenylene ring, whereas the ROT–2Cl attains a single stable equilibrium structure with ϕ = 0.61π. Therefore, the rotational-PES-scanning calculations were carried out here only for the crystalline ROT–2F molecular compass by employing the *Gaussian–external* methodology with SCC–DFTB scheme as an external program. Since the rotational PES of the present concern represents the mathematical relationships between the *Eigen* values *E* of the crystalline molecular assembly and their 3D unit-cell geometries constrained to the specific dihedral angle ϕ (*Gaussian* Keyword: *ModRedundant*) suitable to rotate the central phenylene unit manually in respect to the static siloxaalkane arms, the priory optimized unit-cell structure **B** (ϕ = 0.44π) was taken as an initial input geometry, and computed the concerned *Eigen* value at each fixed ϕ explicitly under "PBC + Dispersion Energy corrections" features of the DFTB: the value of ϕ = 0.44π was consecutively decreased and increased up to 0π and 2π by anticlockwise

(– decrement) and clockwise (+ increment) PES–scanning techniques respectively. The particular value of E at each fixed ϕ was graphically plotted as shown in Figure 6, where the theoretically traced two degenerate equilibrium structures of the ROT–2F related to each other by 1π difluorophenylene flipping are represented by β and β'. The two global minima; structure **B** (β position; E = –704.278668 E_h) at ϕ = 0.44π, and structure **B'** (β' position; E = –704.278668 E_h) at ϕ = 1.44π located on the PES represent the 1π–flipped (0.44π↔1.44π) structures (positions) of the unit-cell (difluorophenylene rotators) which are found to be structurally closed (in terms of the unit-cell geometrical parameters and their molecular alignments), orientationally equivalent (in terms of the siloxaalkane cage structure and its peripherally aligned arms), and positionally rotated (in terms of the difluorophenylene ring's alignment to the spin axis and the static peripheral spokes) to each other. The corresponding unit-cell structures derived through the X–ray diffraction techniques have exactly same type dihedral angle as ϕ=0.56π, and ϕ =1.57π respectively (1π–flipped (0.56π↔1.57π) positions of the difluoro-phenylene rotator). Towards acquiring more in-depth theoretical clarifications and justifications of this 1π-flipping motion such as temporal rotary motion/dynamics at real time, and confirming its experimentally reported plus the *Gaussian–external* predicted 1π–flipped degenerate positions β and β', present authors have currently proceeded NCC–DFTB type molecular dynamics (hereafter, MD) simulation studies under PBC at different kinetic temperatures T = 273K, 300K, 600K, and 1200K. Due to being the MD simulation procedure complex, tedious, and time consuming, no dispersion energy correction algorithms and self-consistent-charge (SCC) computations of the DFTB are implemented computationally. We expect that the NCC–DFTB MD trajectories may reveal flipping dynamics of the rotator including its average lifetimes for the 1π flipping from $\beta \leftrightarrow \beta'$, & vice-versa, and the

corresponding flipping rates (κ) at wide ranged kinetic temperatures. The κ term that relates mathematically with the E_a *via* Arrhenius equation eventually allows us to estimate the latter quantitatively; ultimately useful to justify the *Gaussian–external* predicted E_a.

Besides utilizing rotational PES (Figure 6) for theoretical validations of the

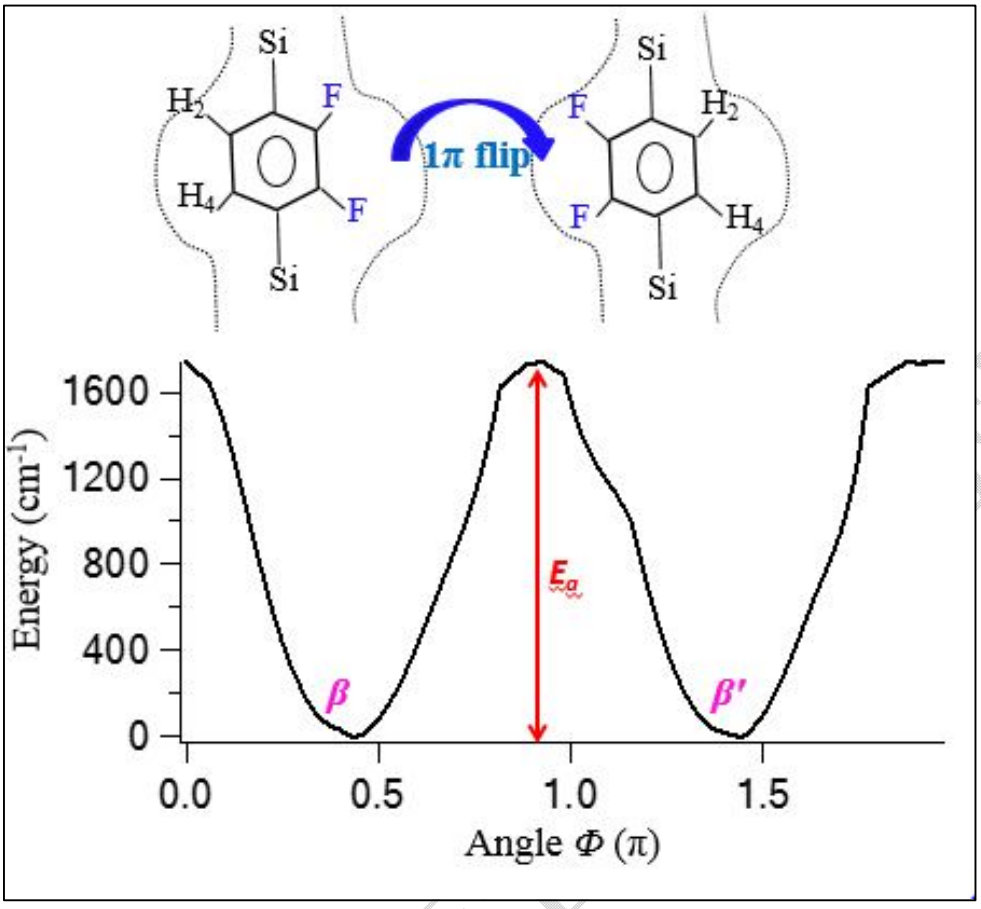

Fig.6. The *Gaussian-external* methodology with "DFTB + PBC + dispersion energy correction" derived rotational potential energy surface (PES) of the molecular compass ROT–2F. The symbols $\boldsymbol{\beta}$ and $\boldsymbol{\beta'}$ represent two degenerate equilibrium positions of the central rotating segment (difluorophenylene), and $\boldsymbol{E_a}$ notifies the rotational energy barrier ($\boldsymbol{E_a}$ = *1700cm*$^{-1}$ = 4.86 kcal/ mol.). The corresponding 1π flipped positions of the difluorophenylene segment inside the siloxaalkane spokes (symbolized by the dotted curves) are demonstrated in the inset.

experimentally predicted degeneracies, we use it here to find the exact magnitude of the energy barrier E_a required to be overcome by the $\boldsymbol{\beta}$ in the course of flipping into $\boldsymbol{\beta}'$ position or vice-versa. The E_a is observed as 1700 cm^{-1} (4.86 kcal/mol.); a significantly larger value than that estimated for its molecular analogue ROT–2H (E_a = 420 cm^{-1} (1.2 kcal/mol.)) [11] is because of the stronger steric interactions between the two F atoms attached to the ROT–2F's phenylene ring themselves and with the surrounding siloxaalkane spokes (intramolecular type) plus the

interactions between the dipolar rotators themselves of the neighboring molecules, and many other van Der Waal's force type nonbonding interactions between the periodically arranged molecules in the crystalline lattice. However, the same E_a is found to be much lower than that reported for the previously synthesized molecular gyroscopes with fluorine-substituted and non-substituted phenylene rotators encapsulated inside the various other types of static frameworks [19]. For example, the E_a values for 1,4-bis-(3,3,3-triphenylpropynyl)-2-fluorobenzene (rotator: fluorobenzene); 1,4-bis-(3,3,3-tri- phenylpropynyl)-2,3-difluorobenzene (rotator: difluorobenzene); platinum dihydride (rotator) complex with two bulky *trans* disposed phosphine (stator) type molecular gyroscopes were reported as 12–14 kcal/mol. [5], 14–15 kcal/mol. [19, 31], and 3.0 kcal/mol. [19] respectively. The in-depth critical analyses and the associated quantitative explanations related to the theoretically estimated E_a values for the different types crystalline molecular gyroscopes/compasses synthesized in between the years: 2002–2020, are concisely presented in the latest review article published elsewhere [19], where the theoretical investigations of the crystalline molecular gyroscope ROT–2H (a synthetic precursor molecular analogue for ROT–2F, and ROT–2Cl) reported by our groups in 2012 [11] are cited by underscoring the reasons underlying exceptionally lower E_a value. Therewith, the exceptionally better molecular architectures, and the structural topologies adopted for the ROT–2H with using robust type Si–O based peripheral arms are recognized as unique among the gyroscopes synthesized since 2002. Based on these evidences /analogies, the ultimate conclusion we derive here is the ROT–2H or its molecular analogue ROT–2F has a far better siloxaalkane type frameworks aligned peripherally with attaining completely closed structural topology suitable for exhibiting gyroscopic/compass-needle functions facilely: the three flexible yet robust type explicit siloxaalkane arms designed around the difluoro-substituted or unsubstituted phenylene

units behave as the most potential means of blocking the steric effects of the neighboring molecules as well as their dipolar or non-polar rotators efficiently. Reiterating the same, the utmost credit for lowering the E_a value goes to the atypical type experimental synthesis, unique strategical designation & molecular architectures of aligning three robust yet flexible explicit siloxaalkane arms peripherally due to which significantly weaker steric interactions between the (a) central dipolar rotator and the surrounding siloxaalkane arms, (b) the arms themselves, and (c) the molecules present in each unit-cell of the ROT–2H /ROT–2F/ROT– 2Cl exists. Nevertheless, the structural topologies, crystalline environment, and the structurally dependent rotary descriptors are the most responsible factors for deciding whether the specific molecular gyroscopes/compasses undergo smooth/hindered type flipping motion or not, and sometime prevented at ordinary temperatures. One of the most important yet quite supportive reasons why the principal investigators/potential researchers/original and review papers' authors around the world have given the special stresses on the importance of deriving rotational PESs of the crystalline molecular gyroscopes/compasses with the deterministic E_a by addressing all the possible non-bonding type interactions is due to a substantial correlation between the strategical designation/laboratorial synthesis of the crystalline molecular gyroscopes/compasses and their facile rotary motion: the more closure the structural topology, the more smaller is the E_a, and eventually far better is the molecular architectures & experimental/computational prototype designations. Towards many other astonishing perspectives involving molecular designing/ architecting strategies, laboratorial syntheses, functionalization efficiencies of the Si–O–Si linkages and the thermal stability & structural robustness of the Si–O bonds and their chains & segments used in each siloxaalkane arm, and externally controlled rotary motion of the dipolar rotators, the theoretical investigations/interpretations acquired herewith for the ROT–2F and

ROT–2Cl favor all the indispensable scenarios required to unlock a new innovation arena in the molecular machinery world.

Lastly, all the theoretically derived molecular geometries and energetics plus their mathematical or graphical relationships in the form of PES for the giant macrocyclic crystalline molecular assemblies ROT–2F and ROT–2Cl by addressing almost all types of their nonbonding or noncovalent type interactions such as dipole-dipole, London dispersion, ion–dipole and ion induced dipole forces, dipoles-induced dipoles forces, electromagnetic forces of attraction or repulsion, and many other secondary type forces that mediate the interactions between the molecules, etc. along with incorporating all the periodically arranged molecular networks and their unit-cells verified the *Gaussian-external* methodology as a versatile yet efficient (gains two order of magnitude in speed) quantum mechanical means. This novel computational mean and the entire theoretical perspectives would be the most predominant supportive evidences for advancing and promoting the DFTB+ scheme operated through the *Gaussian–external* in performing large scale structural and dynamical analyses under extremely low computational resources platforms.

4. Conclusion

This theoretical research work was mainly aimed at computing Crystal structures, Molecular energetics, and Potential Energy Surface (PES) of the experimentally synthesized amphidynamic and non-amphidynamic type crystalline molecular gyrotops encapsulating mobile (rotator) and immobile dihalo-substituted dipolar phenylene units respectively into the chemically identical siloxaalkane spokes (stator). The experimentally (X–ray diffraction) observed facile flipping motion of the centrally encapsulated difluoropheylene (compass-needle) segment of the crystalline siloxaalkane molecular compass ROT–2F, and its two degenerate 1π-

flipped positions actually triggered us for accepting it here as a subject of the major concern. In contrary, the non-amphidynamic siloxaalkane molecular crystal ROT–2Cl showing no flipping motion of its dichlo-rophenylene segment made us to take it as a reference molecular crystal. In the course of clarifying their experimentally/theoretically observed facts, the priory predicted structural as well as dynamical assets of their molecular analogue and synthetic precursor module ROT–2H having a nonsubstituted phenylene unit surrounded peripherally by the exactly same type spokes were referred time to time. Based on the current research interests and the primary objectives set for this study, the *Gaussian–external* methodology with SCC–DFTB scheme (external program) offering "Periodic boundary condition (PBC) + Dispersion energy corrections" calculations was employed, and implemented their most essential features by utilizing a standardized interface of the former. Actually, due to being ROT–2F & ROT–2Cl crystals the massive molecular assemblies with 780 (orthorhombic, number of molecules = 4) and 390 (orthorhombic, number of molecules = 2) atoms per unit-cell at 273K respectively, the electronic structure calculations offered by the *Gaussian* package was computationally expensive, and were hardly terminated with specific *Eigen* values and equilibrium unit-cell structures under PBC. Besides this, the *Gaussian* calculations addressing "Dispersion energy corrections" under PBC were far from fail-safe. Towards these failures, we though recognized the SCC–DFTB approach a computationally superb model, it lacks the features as similar as *Gaussian's* "*ModRedundant*": the focal computational means of this studies through which the relaxed PES, energy barrier E_a & associated rotary dynamics, and experimentally observed 1π–flipped degenerate equilibrium structures **B** and **B'** of the ROT–2F were required to be determined. Therefore, we adopted *Gaussian–external* methodology linked to the SCC–DFTB scheme *via* the user's external script, and employed all the essential theoretical features computationally.

We at first evaluated all the X–ray derived equilibrium structures **B** and **B'** of the ROT–2F & a single stable structure of the ROT–2Cl, and characterized their unit-cells explicitly on the bases of predetermined structural parameters (bond lengths, bond angles, dihedral angles, free-volumes units, etc.). We found very minimal structural disorders in between the experimentally and theoretically produced unit-cell structures of both ROT–2F and ROT–2Cl crystals in respect to their siloxaalkane cage deformations, positional alignment of the central dihalo-substituted phenylene units, peripheral distributions of each siloxaalkane arm, distance between the central rotator and the O atom of each arm $d_{CO}\{d_1, d_2, d_3\}$ (free–volume units), etc. The significant abnormalities we noted more especially in the Si–O bond lengths and Si–O–Si bond angles associated with $-(Si-O)_x-$ segments & −Si–O− linkages of each siloxaalkane arm of each theoretically optimized unit-cell structure; however, were interpreted as quite satisfactory based on the actual mathematical formalisms and quantum mechanical approximations used in the DFTB while addressing the covalent and ionic characters of the chemical bonds (the Si–O bonds have 75% covalent and 25% ionic characters). The detailed analyses of the $d_{CO}\{d_1, d_2, d_3\}$ datasets measured for every unit-cell structures confirmed the maintenance of enough intervening space in between the O atom of each siloxaalkane arm and the phenylene *ortho* carbon holding halogen atoms (free–volume units) even in the theoretically derived unit-cell structures as well as the presence of structural deformation to some extent; validating themselves with the experimentally produced structures of ROT–2F and ROT– 2Cl. The relatively stronger steric effect experienced by the peripheral siloxaalkane arms themselves, and by the centrally located dihalo-substituted dipolar rotators, the intense intermolecular interactions between the molecules arranged periodically in the crystalline state, the considerable dipole-dipole interactions, etc. were recognized as the most significant nonbonding factors deterministic for

creating the rotary obstructions (rotational energy barrier, E_a) responsible for exhibiting facile, hindered, or prevented flipping as in ROT–2H, ROT–2F, and ROT–2Cl respectively; eventually provoking the chemists for adopting compatible laboratorial and computational pathways for designing topologically closed molecular gyrotops. For the crystalline molecular compass ROT–2F, we derived rotational PES with respect to its static siloxaalkane arm, and estimated its E_a value as 1700 cm^{-1} (4.86 kcal/mol.); an extremely essential energy scale for approximating the net energy required to be overcome by its rotator while exhibiting 1π–flipping motion between **B** and **B'**, which in fact is always taken as an indispensable indicator towards deciding whether the concerned crystalline molecular compasses/gyroscopes can be functionalized at ambient temperatures or not. The same PES was used in order to trace out the two degenerate global minima positions where the respective dihedral angles and *Eigen* values were found as *Th.* 0.44π (*Exp.* 0.56π) & *Th.*1.44π (*Exp.*1.57π) radians (0.44π ↔ 1.44π;1π flip), and –704.278668 (E_h) & –704.278668 (E_h) Hartrees; reassured the experimentally observed 1π-flipped degenerate equilibrium structures **B** and **B'**. We verified this energetic degeneracy through the Van't Hoff equation, & equation of Gibbs free energy, and reconfirmed their experimentally reported 50:50 site occupancy factors & identical number densities at 273K. In order to materialize these theoretically predicted amphidynamic features of the crystalline ROT–2F, and to realize its real-time 1π-flipping motions at wide ranged kinetic temperatures, we are currently employing computationally cheap NCC–DFTB MD simulations by considering the size of its unit-cell, crystallinity, and the available computer resources.

References

1. Tejedor RE, Blanco LR, Closa JT. Multiscale modeling for complex chemical systems: Highlights about the Nobel Prize in Chemistry 2013. AFINIDAD LXXI. 2014; 566:1–6.
2. Magalhaes AL. Gaussian-Type Orbitals versus Slater-Type Orbitals: A Comparison. Journal of Chemical Education. 2014; 91:2124−2127.
3. Marahatta AB. Advanced Computer Graphics Aided Molecular Visualization and Manipulation Softwares: The Hierarchy of Research Methodologies. International Journal of Progressive Sciences and Technologies. 2023; 36(2):136–160.
4. Foresman JB. Frisch Æ. Exploring Chemistry with Electronic Structure Methods, 3rd ed., Gaussian, Inc.: Wallingford, CT, 2015.ISBN: 978-1-935522-03-4.
5. Frisch MJ, Trucks GW, Schlegel HB, Scuseria GE, Robb MA, Cheeseman JR, Scalmani G., Barone V., Petersson G A, Nakatsuji H, Li X, Caricato M, Marenich A, Bloino J, Janesko BG *et al*. Gaussian 09, Revision A.02; Gaussian, Inc.: Wallingford, CT, 2016.
6. Foresman JB. Frisch Æ. Exploring Chemistry with Electronic Structure Methods, 2nd ed., Gaussian, Inc.: Pittsburgh, PA, 1996.ISBN: 978-0963676931.
7. Seifert G. Tight-Binding Density Functional Theory: An Approximate Kohn−Sham DFT Scheme. Journal of Physical Chemistry A. 2007; 111(26):5609–5613.
8. Zheng G, Irle S, Morokuma K. Performance of the DFTB method in comparison to DFT and semiempirical methods for geometries and energies of C_{20}–C_{86} fullerene isomers. Chemical Physics Letter. 2005; 412(1–3):210–216.
9. Aradi B, Hourahine B, Frauenheim Th. DFTB+ a Sparse Matrix-Based Implementation of the DFTB Method. Journal of Physical Chemistry A. 2007; 111(26): 5678–5684.

10. Elstner M, Porezag D, Jungnickel G, Elsner J, Haugk M, Frauenheim Th, Suhai S, Seifert G. Self-consistent-charge density-functional tight-binding method for simulations of complex materials properties. Physical Review B. 1998; 58:7260–7268.
11. Marahatta AB, Kanno M, Hoki K, Setaka W, Irle S, Kono H. Theoretical Investigation of the Structures and Dynamics of Crystalline Molecular Gyroscopes. Journal of Physical Chemistry C. 2012; 116:24845–24854.
12. Marahatta AB, Kono H. Performance of NCC- and SCC-DFTB Methods for Geometries and Energies of Crystalline Molecular Gyroscope. International Journal of Innovative Research and Advanced Studies. 2019; 6(5):180–185.
13. Setaka W, Ohmizu S, Kabuto C, Kira M. A Molecular Gyroscope Having Phenylene Rotator Encased in Three-Spoke Silicon-Based Stator. Chemistry Letter. 2007; 36:1076–1077.
14. Setaka W, Ohmizu S, Kira M. Molecular gyroscope having a halogen-substituted *p*-phenylene rotator and silaalkane chain stators. Chemistry Letter. 2010; 39:468–469.
15. Setaka W, Yamaguchi K. Thermal modulation of birefringence observed in a crystalline molecular gyrotop. Proceedings of the National Academy of Sciences of the USA. 2012; 109:9271–9275.
16. Marahatta AB, Kono H. SCC-DFTB Study for the Structural Analysis of Crystalline Molecular Compasses. Chemistry Research Journal. 2022; 7(4):77–94.
17. Dominguez Z, Dang H, Strouse MJ, Garcia-Garibay MA. Molecular compasses and gyroscopes. III. Dynamics of a phenylene rotor and clathrated benzene in a slipping-gear crystal lattice. Journal of American Chemical Society. 2002; 124(26):7719–7727.

18. Balzani V, Venturi M, Credi A. Molecular Devices and machines: A Journey into the Nano World, Wiley-VCH: Weinheim, 2003.

19. Ehnbom A, Gladysz JA. Gyroscopes and the Chemical Literature, 2002–2020: Approaches to a Nascent Family of Molecular Devices. Chemical Reviews. 2021; 121:3701–3750.

20. Horansky RD, Clarke LI, Price JC, Khuong TV, Jarowski PD, Garcia-Garibay MA, Dielectric response of a dipolar molecular rotor crystal. Physical Review B. 2005; 72: 014302-1–014302-5.

21. (a) Macrae CF, Edgington PR, McCabe P, Pidcock E, Shields GP, Taylor R, Towler M, van de Streek J, Mercury: visualization and analysis of crystal structures. Journal of Applied Crystallography. 2006; 39:453–457. (b) Jmol: An open-source Java viewer for chemical structures in 3D. *http://www.jmol.org/*

22. DFTB^{+} Version 1.3 USER MANUAL. *https://dftbplus.org/fileadmin/DFTBPLUS/public/dftbplus/latest/manual. pdf*

23. Koehler C, Hajnal Z, Deak P, Frauenheim Th, Suhai S. Theoretical investigation of carbon defects and diffusion in α-quartz. Physical Review B. 2001; 64:085333-1–085333-7.

24. Marahatta AB, Kono H. Performance of NCC- and SCC-DFTB Methods for Geometries and Energies of Crystalline Molecular Gyroscope. International Journal of Innovative Research and Advanced Studies. 2019; 6(5):180–185.

25. Marahatta AB, Kono H. Structural Characterization of Isolated Siloxaalkane Molecular Gyroscopes via DFTB-based Quantum Mechanical Model. International Journal of Innovative Research and Advanced Studies. 2021; 26(1):526–541.

26. Kang YK, Jhon MS. Additivity of atomic static polarizabilities and dispersion coefficients. Theoretica Chimica Acta. 1982; 61:41–48.

27. Miller KJ. Additivity methods in molecular polarizability. Journal of American Chemical Society. 1990; 112:8533–8542.

28. Elstner M, Frauenheim TH, Kaxiras E, Seifert G, Suhai S. A Self-Consistent Charge Density-Functional Based Tight-Binding Scheme for Large Biomolecules. Physical Status Solidi B. 2000; 217(1):357–376.

29. Pauling L. The nature of silicon-oxygen bonds. American Mineralogist. 1980; 65:321–323.

30. Fujiki M, Koe JR, Terao K, Sato T, Teramoto A, Watanabe J. Optically Active Polysilanes. Ten Years of Progress and New Polymer Twist for Nanoscience and Nanotechnology. Polymer Journal. 2003; 35:297–344.

31. Horansky RD, Clarke LI, Price JC, Karlen SD, Jarowski PD, Santillan R, Garcia-Garibay, MA. Physical Review B. 2006; 74:054306-1–054306-12.